

No Excess of RR Lyrae Stars in the Canis Major Overdensity

Cecilia Mateu¹ and A. Katherina Vivas

*Centro de Investigaciones de Astronomía (CIDA), Apartado Postal 264, Mérida 5101-A,
Venezuela*

cmateu@cida.ve, vivas@cida.ve

Robert Zinn and Lissa R. Miller

*Department of Astronomy, Yale University, PO Box 208101, New Haven, CT 06520-8101,
USA*

robert.zinn@yale.edu, miller@astro.yale.edu

and

Carlos Abad

*Centro de Investigaciones de Astronomía (CIDA), Apartado Postal 264, Mérida 5101-A,
Venezuela*

abad@cida.ve

ABSTRACT

Our multi-epoch survey of ~ 20 sq. deg. of the Canis Major overdensity has detected only 10 RR Lyrae stars (RRLS). We show that this number is consistent with the number expected from the Galactic halo and thick disk populations alone, leaving no excess that can be attributed to the dwarf spheroidal (dSph) galaxy that some authors have proposed as the origin of the CMa overdensity. If this galaxy resembles the dSph satellites of the Milky Way and of M31 and has the putative $M_V \sim -14.5$, our survey should have detected several tens of RRLS. Even if $M_V \lesssim -12$, the expected excess is $\gtrsim 10$, which is not observed. Either the old stellar population of this galaxy has unique properties or, as others have argued before, the CMa overdensity is produced by the thin and thick disk and spiral arm populations of the Milky Way and not by a collision with a dSph satellite galaxy.

¹Also at Universidad Central de Venezuela, Caracas

Subject headings: stars: variables: other, Galaxy: stellar content, Galaxy: structure

1. INTRODUCTION

The Canis Major overdensity was discovered by Martin et al. (2004a) as an excess in the density of 2MASS M-giant stars in the direction $(l, b) = (240^\circ, -8^\circ)$ compared to similar fields in the northern galactic hemisphere. It is estimated to span ~ 100 sq.deg. on the sky and to be concentrated at a distance of ~ 7.2 kpc from the Sun (Martin et al. 2004b; Bellazzini et al. 2006). The large numbers of M-giant and red clump (RC) stars in the CMa overdensity suggest that its main population is of intermediate age ~ 7 Gyr (Bellazzini et al. 2004). A "Blue Plume" of stars in the color-magnitude diagram (CMD) has been interpreted by Bellazzini et al. (2004) and Martínez-Delgado et al. (2005) as the main-sequence of a younger population (age $\lesssim 1$ Gyr)

The CMa overdensity was interpreted by Martin et al. (2004a) as the remnant core of a disrupting dwarf galaxy. However, its origin remains a topic of considerable debate. The dwarf galaxy hypothesis has been contested by several authors who, using different tracers and techniques, have proposed that the overdensity is produced by the stellar populations of the warped Galactic thin disk (Momany et al. 2004), the thick disk (Carraro et al. 2008), and the outer Norma-Cygnus spiral arm (Moitinho et al. 2006; Carraro et al. 2005). Counter arguments have been made by Martin et al. (2004b, 2005) and Bellazzini et al. (2006), in support of the dwarf galaxy nature of CMa, claiming that the Galactic warp is not sufficient to account for the overdensity. The proper motions of a sample of blue plume stars have been measured by Dinescu et al. (2005), who concluded that these stars do not have the space motions expected of galactic stars, if they have the same radial velocity as the sample of M-giants that Martin et al. (2004b) attributed to the CMa dwarf galaxy.

The lack of consensus on this issue is probably a consequence of our limited knowledge of the complex Galactic structure in this direction and also the large and highly variable interstellar extinction. CMa lies in the third Galactic quadrant where the warp of the thin disk has its maximum amplitude (at $l \sim 270^\circ$, Momany et al. 2004; López-Corredoira 2006) and where the Galactic thick disk might be warped as well (Carraro et al. 2008). Also, in this quadrant the spiral arms have not been traced as well as in other directions (Carraro et al. 2005; McClure-Griffiths et al. 2005).

In Table 1, we summarize the previous studies of the stellar populations in the CMa overdensity. Most are photometric and use techniques such as main sequence (MS) fitting

and modelling of either Hess diagrams (HD) or CMDs to obtain the age, metallicity and distance for the stellar population of the CMa overdensity. Carraro et al. (2005); Moitinho et al. (2006); Carraro et al. (2008) and Powell et al. (2008) have made use of multiband photometry and two color diagrams (TCD) to reduce the effects of reddening. The top part of the table shows the studies of the young population in the region, while the bottom part indicates the intermediate age ones. As one can see from the table, no old population ($\gtrsim 10\text{Gyr}$) has been identified.

In summary, there are two conflicting views of the nature of the CMa overdensity:

- The CMa overdensity is a dSph galaxy undergoing tidal disruption. The stellar population of this galaxy is dominated by an intermediate-age population, and there is a minority population of much younger stars (Martin et al. 2004a,b; Bellazzini et al. 2006; Martínez-Delgado et al. 2005).
- The overdensity in the intermediate-age population is produced by a projection of the warped thin and thick disks (Momany et al. 2004; López-Corredoira 2006; Carraro et al. 2008) into the line of sight. The young population corresponds to the outer part of the Norma-Cygnus spiral arm which, being part of the thin disk, also follows the warp (Carraro et al. 2005; Moitinho et al. 2006; Conn et al. 2007).

The goal of our work was to conduct a large scale survey of RR Lyrae stars (RRLS) in order to trace the oldest stellar population ($\gtrsim 10\text{Gyr}$)¹. Old stellar populations containing RRLS have been identified in every dSph satellite of the Milky Way (MW) and of M31 that has been properly surveyed (see e.g. Vivas & Zinn 2006). If the CMa galaxy is similar to these systems in its stellar mix and has the proposed luminosity, a large excess (> 100) of RRLS is expected (see §4). Because RRLS are excellent standard candles, the distances to individual RRLS can be obtained with high precision ($\lesssim 10\%$). If there is a dSph galaxy at a distance of ~ 7.2 kpc (Martin et al. 2004a), an overdensity of RRLS is expected at magnitudes $V \sim 15$. The detection of an overdensity of RRLS that spans a narrow range of magnitudes would be conclusive proof that a dSph galaxy produces the CMa overdensity. On the other hand, the absence of an excess of RRLS would weaken the dwarf galaxy hypothesis, leaving more likely a Galactic origin for the CMa overdensity.

¹Earlier progress reports of our survey can be found in Mateu et al. (2006, 2007)

2. PHOTOMETRIC OBSERVATIONS

The large field of view ($2^{\circ}2 \times 2^{\circ}3$) provided by the QUEST-I camera (Baltay et al. 2002), installed on the 1m Jurgen Stock Telescope at the Venezuelan National Observatory of Llano del Hato, made this an ideal instrument to conduct a large-scale, multi-epoch survey of an extended structure such as the CMa overdensity. The observations were made in the V band and were obtained in two runs during 2004 and 2005, centered at $l \simeq 240^{\circ}$, $b \simeq -9.5^{\circ}$ and spanning ~ 30 sq. degrees with an effective coverage of ~ 20 sq. deg. (which takes into account the area missed because of the gaps between the CCDs in the mosaic camera and the saturation of very bright stars). On average, we obtained ~ 19 epochs per field in 24 nights, with a time spacing between consecutive observations ranging from a few hours up to several weeks. Infrared J, H and K magnitudes from the 2MASS catalogue were also obtained for each star.

The area covered by our survey and previous studies is shown in Fig. 1, where a schematic diagram is overlaid on an extinction map derived from the Schlegel et al. (1998) dust maps. The CMa feature spans ~ 100 sq. deg. and has a smoothly varying density across the plane of the sky, which according to Martin et al. (2004a) can be fitted with Gaussian profiles. The axes of the ellipse shown in Fig.1 correspond to the full-width at half maxima (FWHM) derived for CMa using the aspect ratio of $\sim 5 : 1$ and the FWHM in the latitude direction measured by Butler et al. (2007). Assuming a Gaussian profile with these FWHM we computed that $\sim 3\%$ of the stars in CMa overdensity should be present in our survey’s footprint. The percentage could be smaller than this because Butler et al. (2007) considered $5 : 1$ to be a lower limit of the aspect ratio. From Fig. 6 of Martin et al. (2004a), we estimate that the aspect ratio is probably not much larger than $\sim 6 : 1$, and consequently, that our survey’s coverage is $\gtrsim 2\%$. In the following discussion, we adopt 2% to be conservative. As shown in Fig. 1, our survey includes the same central regions where others (e.g., Martinez-Delgado et al. 2005; Bellazzini et al.2006; Butler et al. 2007) have detected large overdensities of stars. One can also see that the extinction is highly variable in the vicinity of CMa and that its main body is located in a low extinction window, as noted by Rocha-Pinto et al. (2006).

2.1. Image Reduction, Photometry and Astrometry

The image frames were reduced using standard *IRAF*² routines for bias subtraction and flat-fielding. Due to the low galactic latitude of the surveyed region, the fields are highly crowded, thus requiring the computation of magnitudes through PSF photometry. The PSF photometry was obtained using *DAOPHOT* tasks with a model PSF spatially variable to second order, constructed from $\sim 130 - 150$ stars per image.

The astrometric solution was computed for each image using the program CM1 (Stock 1981), which calculates the astrometric matrix based on the coordinates of ~ 150 catalogue stars per image, identified from the USNOB1.0 catalogue (Monet et al. 2003). The precision of the obtained astrometric solutions was $0''.18$, which was calculated by matching the coordinates of all objects with the 2MASS point source catalogue, and corresponds to the mean difference between the CM1 and the 2MASS coordinates for each object. This precision is sufficient for identifying each star in the different observations.

2.2. Photometric Calibration and Extinction Correction

The photometric calibration was made in two steps, the normalization of the instrumental magnitudes with respect to a reference night, and the calibration of the reference night photometry using secondary photometric standards.

In the first step, the magnitude zero-point of each night with respect to the reference night was obtained by calculating a 3-sigma clipped mean of the magnitude differences of the stars that were detected on both nights. The use of ~ 2000 stars in the calculations made these zero-points statistically robust. The obtained zero-point was then added to the instrumental magnitudes of all the objects observed on that particular night. At the completion of this process, mean photometric errors were evaluated as a function of magnitude by calculating the standard deviation of the multi-epoch observations of each object. A typical plot of standard deviation σ of PSF magnitudes as a function of the mean magnitude is shown in Fig. 2.

For the second step, observations of the secondary standard fields were made with the 1.3m telescope of the SMARTS consortium at the Cerro Tololo Interamerican Observatory (CTIO), Chile, with the 2048×2048 pixel Fairchild 447 CCD camera, which has a field

²IRAF is distributed by the National Optical Astronomy Observatories, which are operated by the Association of Universities for Research in Astronomy Inc., under cooperative agreement with the National Science Foundation

of view of $6' \times 6'$. The observations were made in the R and V filters on 2004 January 23, under photometric conditions. A field containing Landolt standards was also observed during the night at different airmasses. The photometric solution for the night was applied to the objects detected in the secondary standard fields. The 316 stars that were selected as secondary standards have photometry in both filters and photometric errors ≤ 0.015 magnitudes.

The secondary standards fields were chosen to be centered on open clusters lying in the region, to ensure having blue stars among the secondary standards. Consequently, the color distribution of the 316 secondary standards was quite broad, $0.1 < V - R < 0.8$. Each row of CCDs in the QUEST camera was calibrated independently. The mean *rms* of the calculated solutions is 0.03 magnitudes.

The limiting magnitude obtained is $V_{lim} = 19.5$, defined as the typical magnitude of objects with $\sigma = 0.1$ mag. The completeness magnitude obtained is $V_{com} = 18.5$, which corresponds to the mode of the magnitude distribution of all objects. Finally, the saturation magnitude of the survey is $V_{sat} \sim 13.5$. The heliocentric distance range explored by our RRLS survey is therefore $3 \text{ kpc} \leq D_{\odot} \leq 39 \text{ kpc}$ (for the complete sample and assuming $M_V = +0.55$), which clearly includes the distance range of the CMa overdensity ($5 \text{ kpc} \lesssim D_{\odot} \lesssim 10 \text{ kpc}$, see Table 1).

Finally, the extinction correction was performed on a star by star basis, since extinction is highly variable in the surveyed region (as shown in Fig. 1) due to its proximity to the Galactic plane. This was done by subtracting the corresponding A_V at the position of each star, computed from a linear interpolation of the Schlegel et al. (1998) dust maps, and including the asymptotic correction proposed by Bonifacio et al. (2000).

3. RR LYRAE STARS

3.1. RR Lyrae search

The first step in the RRLS search was the identification of stars showing photometric variability in the V magnitude, using the procedure explained in Vivas et al. (2004). This consisted of computing, via a χ^2 test, the probability of the V magnitude dispersion being solely due to the photometric errors. From the catalogue of 286,837 stars, 2775 stars had $P_{\chi^2} \leq 0.001$ which indicates that they have a probability of 99.9% of being variable.

The RRLS search was further restricted to the 651 variable candidates fulfilling the following criteria: (i) intrinsic color indices $(V - J)_0, (V - H)_0, (V - K)_0$ consistent with

those of spectral types earlier than G0. (ii) observed amplitude $\Delta V \geq 0.20$, and (iii) number of observations in the V filter, $n_{obs}^V \geq 10$.

The RRLS search followed the procedure devised by Layden (1998) for fitting the light curves of RRLS. This consisted of fitting light-curve templates while varying four parameters: period, amplitude, phase offset and magnitude at maximum light. For the fits of *RRab* variables, we used the six templates made by Layden (1998), which cover the range of light-curve shapes of this type of star. For *RRc* stars, we used either a cosine curve or a template made by averaging and smoothing the light curves of 10 well-observed *RRc* stars from the QUEST RR Lyrae catalogue (Vivas et al. 2004).

The ranges for the trial parameters were explored according to the known distribution of periods and amplitudes for RRLS of each type (Vivas et al. 2004), using a step of 10^{-5} d for the period in the range 0.4 – 1.2 d for *RRab* and 0.2 – 0.5 d for *RRc*; a step of 0.01 mag for the amplitude in the ranges 0.2 – 1.4 mag for *RRab* and 0.18 – 0.7 for *RRc*; and steps of 0.01 mag and 0.005 for the V magnitude at maximum light and the phase offset respectively. These values were then taken as the uncertainties of the corresponding parameters. For each set of trial parameters, the χ^2 of the fit was computed and finally, the four best fits for each RRLS type were visually inspected for every star. The stars for which an adequate template fit was found were selected as initial RRLS candidates. Additionally, the epoch at maximum light and the flux-averaged V magnitude $\langle V \rangle$ were calculated using the best fitting light-curve parameters.

3.2. Photometric Follow-up

The observations with the Stock telescope yielded for some RRLS candidates poorly sampled light curves. Consequently, we obtained additional observations with the 0.9m, 1.0m and 1.3m telescopes of the SMARTS consortium at Cerro Tololo Interamerican Observatory (CTIO), during Sept-Oct 2004 and Jan-Feb 2008; and with the 1.0m Reflector at the National Observatory of Venezuela (NOV), during Jan 2008. All observations were made in the V filter. This photometry was normalized to the reference night of the QUEST photometry using $\sim 120 - 250$ field stars per image for the CTIO observations and $\sim 70 - 80$ for the NOV observations. On average, 5 additional epochs were obtained for each candidate RRLS, yielding an average 24 observations per star. Light curve parameters were recalculated with the additional observations, including exploration of period aliases. With these additional observations, only 16 stars passed our tests for RRLS candidates, 10 of type *c* and 6 of type *ab*.

3.3. Spectroscopic Follow-up

Spectroscopic follow-up of the 14 brighter ($V < 16.5$, equivalent to $D_{\odot} \lesssim 12$ kpc) RRLS was conducted in order to obtain radial velocities and metallicities. These bright stars lie within the distance range of the CMa overdensity.

Spectra were obtained with the Cassegrain spectrograph at the 1.5m SMARTS telescope in Cerro Tololo Interamerican Observatory, Chile. The observations were obtained in service mode in the months 2004 November-December, 2005 January, and 2008 February. The instrumental setup was the same used by our group to observe a large number of halo RRLS from the QUEST survey. We refer the reader to Vivas et al. (2008) for details on the instrumental setup, data reduction, and methods to estimate radial velocities and metallicities. Here we will summarize only the more important issues. The spectra have a resolution of 4.3 \AA and a spectral range from 3500 to 5300 \AA . Radial velocities were obtained by Fourier cross-correlation (IRAF's *fxcor* task) with several radial velocity standards of the same spectral type. The radial velocity standards were chosen from the list of Layden (1994) which also serve as pseudo-equivalent width standards for estimating the metallicities. Each RRLS was observed twice at different phases during the pulsation cycle. To obtain the systemic velocity, V_{γ} , of each star, the radial velocity curve of the well-studied star X Arietis was fitted to the data (see also Vivas et al. 2005). The metallicities were estimated using the calibration by Layden (1994) of the pseudo-equivalent width of the Ca II K line (W(K)), corrected for interstellar absorption, and the mean pseudo-equivalent widths of the β , γ , and δ Balmer lines (W(H)). The estimated error of the [Fe/H] measurements, which are on the Zinn & West (1984) metallicity scale, is 0.15 dex for the RR*ab* and 0.20 dex for the RR*c*.

3.4. Contaminants of the Sample

Our sample is expected to be contaminated by other types of variable stars. In order of decreasing likelihood, these are contact eclipsing binaries (W UMa stars) of A-F spectral type, pulsating blue straggler stars of the Delta Scuti and SX Phoenicis types, and Cepheids of type II and of the anomalous classification.

In many cases the light curves of W UMa stars resemble a cosine curve (Rucinski 1993), making it difficult to distinguish them photometrically from RR*c* stars, since their period ranges also overlap. However, several orbital configurations do have light curves that can be distinguished, and consequently, we also fitted a W UMa templates to some of the candidate RR*c* stars. This template was constructed from the Fourier coefficients of Rucinski (1993) ($i = 80^{\circ}, q = 0.4, f = 0$), following Layden (1998). We used only this W UMa template, which

we consider representative of the type, since our goal was only to reduce the contamination that these stars introduce in the RRc sample, and not to survey their properties. The W UMa template yielded a better fit than the RRc template for 3 stars, namely 25711, 10651 and 18056. The radial velocities of these stars are also consistent with the interpretation that these stars are not RRLS. The radial velocities of stars 25711 and 10651 appear to be constant, while for star 18056 the radial velocity curve template for RRc stars does not fit the observations properly. Furthermore, the mean velocities of these 3 stars are 81 km s^{-1} , 26 km s^{-1} and 77 km s^{-1} , respectively, which lie close to the radial velocity peak expected for thin disk stars, which for the survey region is $V_\gamma \sim 69 \text{ km s}^{-1}$ with $\sigma V_\gamma \sim 22 \text{ km s}^{-1}$ (see §4.2). We conclude that stars 25711, 10651 and 18056 are most likely eclipsing binaries from the thin disk, and have classified them as W UMa stars.

In the selection of RRLS candidates, we imposed color cuts to exclude the numerous red variables in the fields, but some non-RRLS may pass these criteria. Our spectroscopy revealed that the RRc candidates 6460, 5564, and 17237 have late F spectral types. Since these types are too late for RRc stars (Smith 1995), we have removed them from the sample of candidate RRLS.

The Delta Scuti and SX Phoenicis variables, also known as dwarf cepheids, have spectral types A0-F5 III-V, V amplitudes $< 0.7 \text{ mag}$ and periods in the ranges $0.01 - 0.2 \text{ d}$ and $0.04 - 0.08 \text{ d}$ respectively. Consequently, the period range of Delta Scuti stars overlaps with the short period end of the RRc period distribution (Smith 1995; Kholopov et al. 1998). In the case of SX Phoenicis stars, it is expected that some stars will have period aliases within the range expected for RRc stars, which may escape detection by the low number of epochs and the time spacing of our observations. Although much less numerous than eclipsing binaries, Delta Scuti and SX Phoenicis stars are expected in the Galactic disk and halo respectively, and hence are possible contaminants of the RRc sample.

Finally, a possible contaminant of the RRab sample are Anomalous Cepheids and short period type II Cepheids, also known as BL Herculis and W Virginis stars (Sandage & Tammann 2006; Kholopov et al. 1998). These stars have light curve shapes and period ranges that partially overlap with RRLS stars. However, these stars are very rare in comparison to the RRLS in the halo population, which is the only MW population in which they have been found. Given that the halo population is itself a small contributor to the stellar density in the CMA fields (see §5), the contamination from these stars should be small compared to the other types of stars.

After the removal of the likely contaminants, 10 stars remained in our sample of RRLS candidates. The light curves for the 10 RRLS are shown in Figure 3, and those of the 3 W UMa stars are shown in Figure 4. The light curve and physical parameters obtained

for the 10 RRLS in Table 2, including heliocentric distances of RRLS calculated based on the flux-averaged mean magnitude $\langle V_0 \rangle$ and assuming $M_V^{RR} = +0.55$ (Demarque et al. 2000; Vivas et al. 2001). The uncertainty in the distance to the RRLS has been estimated in 7%, following Vivas & Zinn (2006). The light curve parameters of the rejected RRLS candidates are summarized in Table 3. We must caution, however, that some contamination by non-RRLS may be still present, particularly for the sample of RRc stars.

3.5. Completeness of the Survey

The survey’s completeness was evaluated as the fraction of synthetically generated light curves for which the period was successfully recovered. A total of 3600 synthetic RRLS light curves were generated for both R Rab and RRc types, with 10, 15 and 20 data points and a time sampling characteristic of the survey. Typical random photometric errors were added as a function of magnitude (Fig. 2). The synthetic light curves were used as input for the RRLS identification algorithm described in §3.1. If for a synthetic light curve, the difference between the real and the best fitting period was better than 1%, it was considered as recovered. The percentage of recovered light curves as a function of magnitude for types R Rab and RRc are shown in Fig. 5. For this plot, we averaged the results obtained for light curves with different numbers of data points. One can see from this figure that the average completeness of the survey is $\sim 90\%$.

RRLS 26896 has been previously identified as an RRLS by the All Sky Automated Survey (ASAS-3, Pojmanski 2002). The period derived for this star in the ASAS-3 survey ($P_{ASAS} = 0.39725$ d) coincides with our best-fitting period (see Table 2). The ASAS V-filter observations are systematically brighter than ours, but this is due to a bright neighbor ($V \sim 13.6$) of star RRLS 26896, lying at a distance of $\sim 14''$, which is unresolved in the ASAS survey. This is the only RRLS from the GCVS or the ASAS-3 that lies in the surveyed region, and it was successfully recovered by our survey.

4. EXPECTED NUMBER AND DISTRIBUTION OF GALACTIC RRLS

RRLS are found in the halo and thick disk stellar populations of the MW, and a certain number of them are expected in the region that we have surveyed. Below we estimate the numbers of these stars and their distributions in space and radial velocity to see if there is an excess of RRLS that should be attributed to another source.

4.1. Expected Radial Profile of Galactic RRLS

Since the volume of our survey is naturally expressed in heliocentric Galactic coordinates (D_\odot, l, b) , the number N_{RR} of RRLS in a given volume is expressed as

$$N_{RR} = \int_{D_\odot^o}^{D_\odot^f} \int_{b_o}^{b_f} \int_{l_o}^{l_f} \rho(D_\odot, l, b) D_\odot^2 dD_\odot \cos b db dl \quad (1)$$

This equation requires that the density profile ρ be expressed in terms of heliocentric coordinates. Since the density profiles of the halo and thick disk are naturally written in galactocentric coordinates, the coordinate transformation complicates the integral in Eq.1, making extremely difficult to obtain an analytical solution. Consequently, we solved it numerically by using a Monte Carlo implementation of the Von Neumann Rejection Technique (Press et al. 2002).

The RRLS density profile of the Galactic halo has been well constrained by several authors (e.g. Vivas & Zinn 2006; Wetterer & McGraw 1996). In the case of the Galactic thick disk, the RRLS density profile has only been characterized in the direction perpendicular to the plane of the disk (Layden 1995), which is due to the difficulties in surveying the crowded fields near the Galactic plane where the interstellar extinction is high. The density profile of the thick disk has been studied by several authors using different tracers and techniques (e.g. Brown et al. 2008; Cabrera-Lavers et al. 2005; Larsen & Humphreys 2003), and we have adopted these profiles as valid for the RRLS too. The assumed analytical expressions for the density profiles of the Galactic halo and thick disk are listed in Table 4. In Table 4, we also give the density profile of a hypothetically warped thick disk with the same warp properties as the thin disk. This profile is used in order to explore the possibility that the thick disk might be warped, as suggested by Carraro et al. (2008). Since the possible warp of the thick disk has not been explored in detail, the best assumption we can make is that it is described by the same parameters as the warp of the thin disk (e.g. López-Corredoira et al. 2002). This is a plausible assumption since analytical models of warp formation (Sparke & Casertano 1988) and N-body simulations, which model the formation of warped thin and thick disks (Quinn et al. 1993) predict similar properties.

The profile parameters, namely the RRLS density normalization ρ_\odot^{RR} (for type ab RRLS), the power-law index n and flattening ratio c/a of the halo, as well as the scale length h_R and scale height h_z of the thick disk, determined by several authors using different tracers are presented in Table 5. Since the only determination available to date of ρ_\odot^{RR} for the thick disk is that of Layden (1995), derived from nearby RRLS, we use this value ($\rho_\odot^{RR} = 10 \pm 4$ RRLS/kpc³) in the calculation of N_{RR} using the scale lengths and heights

derived by different authors (Table 5).

By solving Eq. 1 using the profiles given in Table 4, we obtained the total number of RRLS expected in the range $3 \text{ kpc} \leq D_{\odot} \leq 20 \text{ kpc}$. The results are shown in the last column of Table 5, in which N_{RR} has been computed for RRLS of both types by correcting for the factor $N_{ab+c}/N_{ab} = 1.29$ (Layden 1995) to account for RRLS of type c. Also, we derived the number of RRLS as a function of heliocentric distance, which is shown in Fig. 6 together with the observed radial distribution of RRLS in our survey. From Fig. 6, one can see that the theoretical RRLS radial distribution changes only slightly with the different sets of parameters. Most importantly, in the case of the warped thick disk there is a peak located at $\sim 7.5 \text{ kpc}$, independent of the choice of the parameter set. This peak corresponds to the distance where the survey’s line of sight intersects the highest density part of the thick disk’s warp. The existence of this peak in the case of a warped disk is what led Momany et al. (2004, 2006) and others (López-Corredoira 2006; Carraro et al. 2008) to contest the interpretation of the CMa overdensity as a dwarf galaxy remnant, suggesting instead that it could be due to the warped Galactic disk(s).

From Table 5, one can see that 4 – 6 halo RRLS are expected in the distance range of the survey, and 2 – 3 or 3 – 6 RRLS are expected respectively from a normal or warped thick disk. This yields a total of 6 – 9 or 7 – 12 RRLS expected from a Galactic distribution. These numbers are in excellent agreement with the 10 RRLS found in our survey, leaving very little room (if any) for an excess of RRLS over the Galactic background.

To take into account the random fluctuations that are obviously present in such small samples, we made 10^3 random realizations of a halo plus a normal thick disk (H+TD) and of a halo plus a warped thick disk (H+WTD). Each of these realizations was compared with the observed radial distribution, and the probabilities that the distributions are different were computed via a Kolmogorov-Smirnov test. These tests showed that for the H+TD and H+WTD distributions only 4% and 1%, respectively, of the 10^3 realizations were incompatible with the observed distribution (i.e. $P < 0.01$). We conclude, therefore, that the observed RRLS radial distribution is consistent with the expectations from the Galactic models, although the small number of stars hinders any distinction between a normal and a warped thick disk.

Several studies have shown that there is a correlation between the $[\text{Fe}/\text{H}]$ values of RRLS and their memberships in the stellar populations of the MW. Layden (1995), for example, found that the majority of RRLS with $[\text{Fe}/\text{H}] < -1.3$ and $[\text{Fe}/\text{H}] > -1.0$ are members of the halo and thick disk populations, respectively, while the intermediate zone, $-1.3 < [\text{Fe}/\text{H}] < -1.0$, is occupied by a mixture of these populations. According to these limits, the probable memberships of the 8 RRLS in our sample that have $[\text{Fe}/\text{H}]$ measurements are 4 halo stars,

1 thick disk star, and 3 in the mixture zone. While these assignments must be viewed with caution because the $[\text{Fe}/\text{H}]$ distributions of both populations have tails that extend beyond the region of large overlap, they are consistent with the results obtained from the density profiles.

4.2. Comparison with the Observed RRLS Radial Velocity Distribution

As discussed above, we have measured the radial velocities of the 8 RRLS that lie in the distance range of the CMA overdensity ($4 > D_{\odot} > 12$ kpc). In the upper diagram of Fig.7, the radial velocity distributions of the RRab and RRc variables are depicted by the clear and the shaded histograms, respectively. They are plotted separately because the RRc sample is more prone to contamination from other types of stars. In the lower diagram, we have plotted, with arbitrary normalizations, the radial velocity distributions of A-F stars in the halo, thick, and thin disks, as given by the Besançon Galactic model (Robin et al. 2003) for the area of our survey. The halo and thick disk radial velocity distributions correspond to stars in the distance range of the RRLS in our survey; while the thin disk distribution was obtained for stars without any constraint on distance. The thin disk distribution is shown for reference since, as mentioned in §3.4, some contamination may remain and these non-RRLS are most likely members of the thin disk. The dashed lines in the upper plot show the positions of the means of the distribution of each component. From this figure one can see that the observed radial velocity distribution is consistent with the expected halo and thick disk distributions. The radial velocities of some of the stars that we have classified as RRc are consistent with membership in the thin disk, but given the overlap in velocity with the halo and thick disk populations, it not certain that these stars are contaminants rather than true RRLS. In conclusion, it appears that 100% of the sample of RRLS can be explained by the contributions from the halo and thick populations and possible contaminants, and therefore, there is no excess of RRLS that requires another explanation.

Martin et al. (2005) measured the radial velocities of large samples of red clump (RC) and red giant branch (RGB) stars in the CMA overdensity, and found that they define a sequence in a plot of D_{\odot} against V_r (see Figs. 6 & 12 in Martin et al. (2005) and our Fig. 8). Their sample of RGB stars were observed in several two-degree fields that were centered on $l = 240^{\circ}$ and $-4^{\circ}8 > b > -10^{\circ}8$, and most of their sample of RC stars were observed in a field at $(l, b) = (240^{\circ}0, -8^{\circ}8)$. Our RRLS survey encompasses the field where the majority of RC stars were observed, and it overlaps with many of the fields where the RGB stars were observed (see Fig. 1).

In Figure 8, the sequence that is defined by the observations of Martin et al. (2005) is

compared to our RRLS observations. For the measurements of the RC stars, we adopted the mean values of V_r that Martin et al. (2005) list in their Table 2 for different bins in D_\odot . In our plot of these values in Figure 8, the vertical error bars depict the size of the bin in D_\odot (1 kpc for the RC stars), while the horizontal error bars depict the standard deviation of the Gaussians that Martin et al. fit to the velocity peaks. For the RGB stars, we adopted the mean V_r and standard deviation that Martin et al. give for the distance bin of 7.5 – 11 kpc. For the mean distance of these RGB stars, we adopted 8.5 kpc from Fig. 12 of Martin et al. (2005).

Figure 8 shows that several of the RRLS are widely scattered over the $V_r - D_\odot$ plane and that there is loose group at $(V_r, D_\odot) \sim (70 \text{ km s}^{-1}, 10.5 \text{ kpc})$. This group should not given much weight because 3 of the 4 stars are type c, the type most likely contaminated by thin disk interlopers, which would have instead $D_\odot \lesssim 4 \text{ kpc}$. Figure 8 shows that the RRLS are not concentrated on the sequence defined by the observations of Martin et al. (2005). Two RRLS, the type ab variable 882 at $(V_r, D_\odot) = (64 \text{ km s}^{-1}, 6.3 \text{ kpc})$ and the type c variable 39928 at $102 \text{ km s}^{-1}, 10.7 \text{ kpc}$, lie within the velocity and distance ranges of the RC and RGB stars that Martin et al. (2005) attribute to the CMA dwarf galaxy. While this could mean that these RRLS belong to this system, this is not necessarily the case. Members of the Galactic halo population are expected to have a very broad peak in velocity near 200 km s^{-1} and a roughly uniform distribution over the range of distances in Figure 8 (see Figures 6 & 7). Consequently, every RRLS in Figure 8 is a candidate halo star. The behavior of the Galactic thick disk population is depicted by the grayscale in Figure 8, which was obtained from the Besançon model (Robin et al. 2003). Since 882 and 39928 lie within the region expected to contain thick disk stars, it is possible that they belong to this Galactic population or the halo population and not to the CMA dwarf galaxy. Our survey has detected 0 to 2 RRLS that *could* be members of the CMA dSph galaxy

5. THE NUMBER OF RRLS IN DWARF SPHEROIDAL GALAXIES

Out of the 10 RRLS found by our survey, at most 2 could be associated with the CMA dwarf galaxy. This is many fewer RRLS than expected.

In Fig. 9, the number N_{RR} of RRLS in dSph satellite galaxies of the MW and M31 is plotted versus their absolute visual magnitude M_V (data from Siegel (2006), Kuehn et al. (2008) and Greco et al. (2008), and the compilation by Vivas & Zinn (2006)). There is a strong correlation between the observed number of RRLS in a galaxy and its absolute magnitude in the sense that the number of RRLS grows with increasing luminosity. This correlation even holds for the extremely low luminosity satellites Boo, CVn I and II ($M_V \gtrsim$

–8.5). It also holds for the Sgr dwarf which is at present undergoing tidal disruption. If the CMa dSph galaxy follows the same trend and has the estimated $M_V \sim -14.5$ (estimates of the absolute V magnitude range from -14.4 to -14.5 , Martínez-Delgado et al. 2005; Bellazzini et al. 2006), then it is expected to contain ~ 2880 RRLS. Our survey covers $\sim 3\%$ of the galaxy, and therefore, it should have detected ~ 86 RRLS. If CMa is more elongated with aspect ratio of $\sim 6 : 1$, the coverage of our survey would be $\gtrsim 2\%$ and hence $\gtrsim 58$ RRLS should have been detected by our survey. Since the expected number of RRLS is a factor of $\gtrsim 40 - 30$ times greater than the number observed, we can safely reject the hypothesis that the CMa overdensity is caused by a "normal" dSph galaxy with $M_V \sim -14.5$. We can also firmly reject the possibility that the luminosity of this galaxy has been simply overestimated. Note that the trend in Fig. 9 indicates that ~ 600 RRLS are expected in a "normal" dSph with $M_V \sim -12$, which is much fainter than any estimate for the CMa galaxy. Nonetheless, if such a system were present, our survey should have detected ~ 12 RRLS as an excess over the expected Galactic background of RRLS, which is not observed.

It also clear from our survey that the putative CMa dSph galaxy must be unlike any other dSph galaxy in its production of RRLS per unit luminosity. Fig. 9 shows that the dSph galaxy that deviates by the largest amount below the line is the MW satellite Leo I. This was long considered to be an example of a galaxy whose stellar population is completely dominated by an intermediate-age population because there was no clear-cut evidence for an older population (e.g. Lee et al. 1993; Gallart et al. 1999). The recent survey by Held et al. (2001), which discovered 74 RRLS in Leo I, showed that even this exceptional system has an old stellar population containing RRLS. The Leo I galaxy has the lowest specific frequency³ of RRLS ($S_{RR}=1.9$) of any of the 13 dSph galaxies that are brighter than $M_V = -8$ (Vivas & Zinn 2006). If a dSph galaxy of $M_V = -14$ produces the CMa overdensity, the results of our survey suggest that it has $S_{RR} < 0.2$, an order of magnitude smaller than that of Leo I.

6. DISCUSSION AND CONCLUSIONS

The QUEST RR Lyrae survey in the CMa overdensity has yielded the following results:

- Ten RRLS, 6 of type *ab* and 4 of type *c*, were found by our survey, which spans ~ 20 sq. deg. and is centered approximately at $(l, b) = (240^\circ, -9.5^\circ)$. The distance range

³The specific frequency, S_{RR} , is defined as the number of RRLS per unit absolute visual magnitude (M_V) normalized to $M_V = -7.5$ (Suntzeff et al. 1991).

covered by the RRLS is $3 \text{ kpc} \leq D_{\odot} \leq 20 \text{ kpc}$, and 8 out of the 10 RRLS are within the distance range of CMa overdensity ($D_{\odot} < 11 \text{ kpc}$).

- Integration of the density profiles of the Galactic halo and thick disk indicates that within the surveyed region the Galactic halo and thick disk should contribute a total of 6 – 9 RRLS, and if the thick disk is warped like the thin disk, the expected number is 7 – 12 RRLS. These numbers are in good agreement with the 10 RRLS found by our survey; consequently there is no excess of RRLS in the CMa overdensity.
- The radial velocities of 8 out of the 10 RRLS were measured, and their values are consistent with membership in either the Galactic halo or the thick disk populations.
- An analysis of the number of RRLS found in the dSph satellites of the MW and M31 indicates that our survey should have discovered ~ 70 RRLS if the CMa overdensity is produced by a typical dSph galaxy with $M_V = -14.5$, the estimated luminosity of the CMa system. Even if this galaxy is 2.5 magnitudes fainter, which is much lower than any estimate in the literature, the expected excess of RRLS is ~ 12 , which is not observed. The CMa dSph galaxy must have a significantly lower value of the specific frequency of RRLS (S_{RR}) than Leo I, the Local Group dSph that has the lowest measured value.

The hypothesis that the CMa overdensity is produced by a dwarf galaxy is severely constrained by the above results. We have shown that if it is a dSph galaxy, the type favored by the proponents of the hypothesis, then it must be unlike any of the satellite dSph galaxies of the MW and M31. No one has proposed that the putative galaxy is a dwarf irregular because there is no sign of a very young stellar population (age < 100 Myr, e.g. de Jong et al. 2007) or star forming regions associated with the CMa overdensity. Nonetheless, we note that RRLS have been found in every dwarf irregular galaxy of the Local Group that has been adequately searched, and that there is evidence for very old and metal-poor stellar populations in the others (see Clementini et al. 2003; Momany et al. 2005; Mateo 1998, and references therein). These populations have probably produced RRLS that await detection.

According to de Jong et al. (2007), the old stars in the CMD of the CMa overdensity have a mean metallicity of $[\text{Fe}/\text{H}] \sim -1$ and ages in the range 3-6 Gyrs, although they could not constrain the presence of an older population. Clearly, the metals in this intermediate-age population must have come from earlier generations of more metal poor stars. There is no sign of a blue horizontal branch (BHB) in the CMD, and our survey has shown that there are very few, if any, horizontal branch stars in the instability strip. The remaining alternative is that the majority of the oldest and most metal poor HB stars of the CMa galaxy must lie on the red side of the instability strip and are therefore part of the red clump

that is observed in the CMD. However, at low metallicities (i.e. $[\text{Fe}/\text{H}] < -2$) a relatively young age is required to keep the horizontal branch to red side of the instability strip (see, for example, Fig. 9 in Rey et al. 2001). Thus, the CMa dwarf must have started its star formation at a later time than is observed in other dwarf galaxies. This was once thought to be the case for Leo I, but we now know that this was incorrect (Held et al. 2001).

Martin et al. (2004a) have suggested that the globular clusters NGC 1851, 1904, 2298, and 2808 once belonged to the CMa dwarf galaxy. These clusters span a range in horizontal branch type from predominantly blue to predominantly red, although each one contains many BHB stars and at least a few RRLS (Lee et al. 1994; Forbes et al. 2004). The idea that they originated in the CMa dwarf is hard to reconcile with the lack of a BHB in the CMa CMD and our result that there is no excess of RRLS in the CMa overdensity. In other dwarf galaxies that have globular cluster systems (e.g., the Sgr and Fornax dSph galaxies), there are stellar populations in the main body that resemble the ones in the retinues of globular clusters.

In summary, the dwarf galaxy explanation for the CMa overdensity requires that the system be unique among dSph galaxies, and perhaps also dwarf irregulars, in its low production of RRLS. The absence of RRLS in the overdensity is consistent with the alternative viewpoint that a combination of the thin and thick disk and spiral arm populations of the MW produces the CMa overdensity (Momany et al. 2004, 2006; López-Corredoira 2006; López-Corredoira et al. 2007; Carraro et al. 2005, 2008; Moitinho et al. 2006; Powell et al. 2008). However, it does not prove that this alternative is correct, and more research on this question is warranted.

This research was based on observations collected at the Jürgen Stock 1m Schmidt telescope and the 1m Reflector telescope of the National Observatory of Llano del Hato Venezuela (NOV), which is operated by CIDA for the Ministerio del Poder Popular para la Ciencia y Tecnología, Venezuela. The facilities of the 0.9m, 1.0m, 1.3m and 1.5m telescopes of the SMARTS Consortium at CTIO, Chile were also used. C. Mateu acknowledges support from the predoctoral grant of the Academia Nacional de Ciencias Físicas, Matemáticas y Naturales of Venezuela. C. Mateu would also like to thank Gustavo Bruzual and Gladis Magris for helpful discussions during the course of this research. R. Zinn and L.R. Miller were supported by National Science Foundation Grant AST-05-07364. The authors are grateful for the assistance of the personnel, service-mode observers, telescope operators and technical staff at CIDA and CTIO, who made possible the acquisition of photometric and spectroscopic observations at the NOV and SMARTS telescopes. This work has also benefitted from use of the USNOFS Image and Catalogue Archive operated by the United States Naval Observatory, Flagstaff Station (<http://www.nofs.navy.mil/data/fchpix/>).

REFERENCES

- Baltay, C. et al. 2002, *PASP*, 114, 780
- Bellazzini, M., Ibata, R., Monaco, L., Martin, N., Irwin, M. J., & Lewis, G. F. 2004, *MNRAS*, 354, 1263
- Bellazzini, M., Ibata, R., Martin, N., Lewis, G. F., Conn, B., & Irwin, M. J. 2006, *MNRAS*, 366, 865
- Bonifacio, P., Monai, S., & Beers, T. C. 2000, *AJ*, 120, 2065
- Brown, W. R., Beers, T. C., Wilhelm, R., Allende Prieto, C., Geller, M. J., Kenyon, S. J., & Kurtz, M. J. 2008, *AJ*, 135, 564
- Butler, D. J., Martínez-Delgado, D., Rix, H.-W., Peñarrubia, J., & de Jong, J. T. A. 2007, *AJ*, 133, 2274
- Cabrera-Lavers, A., Garzón, F., & Hammersley, P. L. 2005, *A&A*, 433, 173
- Carraro, G., Vázquez, R. A., Moitinho, A., & Baume, G. 2005, *ApJ*, 630, L153
- Carraro, G., Moitinho, A., & Vázquez, R. A. 2008, *MNRAS*, 224
- Clementini, G., Held, E. V., Baldacci, L., & Rizzi, L. 2003, *ApJ*, 588, L85
- Conn, B. C. et al. 2007, *MNRAS*, 376, 939
- de Jong, J. T. A., Butler, D. J., Rix, H. W., Dolphin, A. E., & Martínez-Delgado, D. 2007, *ApJ*, 662, 259
- Demarque, P., Zinn, R., Lee, Y.-W., & Yi, S. 2000, *AJ*, 119, 1398
- Dinescu, D. I., Martínez-Delgado, D., Girard, T. M., Peñarrubia, J., Rix, H.-W., Butler, D., & van Altena, W. F. 2005, *ApJ*, 631, L49
- Forbes, D. A., Strader, J., & Brodie, J. P. 2004, *AJ*, 127, 3394
- Gallart, C., Freedman, W. L., Aparicio, A., Bertelli, G., & Chiosi, C. 1999, *AJ*, 118, 2245
- Greco, C. et al. 2008, *ApJ*, 675, L73
- Held, E. V., Clementini, G., Rizzi, L., Momany, Y., Saviane, I., & Di Fabrizio, L. 2001, *ApJ*, 562, L39

- Irwin, M., & Hatzidimitriou, D. 1995, *MNRAS*, 277, 1354
- Kholopov, P. N., et al. 1998, *Combined General Catalogue of Variable Stars*, 4.1 Ed (II/214A). (1998)
- Kuehn, C. et al. 2008, *ApJ*, 674, L81
- Larsen, J. A., & Humphreys, R. M. 2003, *AJ*, 125, 1958
- Layden, A. C. 1994, *AJ*, 108, 1016
- . 1995, *AJ*, 110, 2288
- . 1998, *AJ*, 115, 193
- Lee, M. G., Freedman, W., Mateo, M., Thompson, I., Roth, M., & Ruiz, M.-T. 1993, *AJ*, 106, 1420
- Lee, Y.-W., Demarque, P., & Zinn, R. 1994, *ApJ*, 423, 248
- López-Corredoira, M., Cabrera-Lavers, A., Garzón, F., & Hammersley, P. L. 2002, *A&A*, 394, 883
- López-Corredoira, M. 2006, *MNRAS*, 369, 1911
- López-Corredoira, M., Momany, Y., Zaggia, S., & Cabrera-Lavers, A. 2007, *A&A*, 472, L47
- Martin, N. F., Ibata, R. A., Bellazzini, M., Irwin, M. J., Lewis, G. F., & Dehnen, W. 2004a, *MNRAS*, 348, 12
- Martin, N. F., Ibata, R. A., Conn, B. C., Lewis, G. F., Bellazzini, M., Irwin, M. J., & McConnachie, A. W. 2004b, *MNRAS*, 355, L33
- Martin, N. F., Ibata, R. A., Conn, B. C., Lewis, G. F., Bellazzini, M., & Irwin, M. J. 2005, *MNRAS*, 362, 906
- Martínez-Delgado, D., Butler, D. J., Rix, H.-W., Franco, V. I., Peñarrubia, J., Alfaro, E. J., & Dinescu, D. I. 2005, *ApJ*, 633, 205
- Mateo, M. L. 1998, *ARA&A*, 36, 435
- Mateu, C. E., Vivas, A. K., Zinn, R., & Miller, L. 2006, in *RMxA Conf. Ser.* 25, ed. C. Abad, A. Bongiovanni, & Y. Guillen (Mexico: RMxA), 18–20

- Mateu, C., Vivas, K., Zinn, R., & Miller, L. 2007, in IAU Symposium, Vol. 241, IAU Symposium, ed. A. Vazdekis & R. F. Peletier, 359–360
- McClure-Griffiths, N. M., Dickey, J. M., Gaensler, B. M., Green, A. J., Haverkorn, M., & Strasser, S. 2005, *ApJS*, 158, 178
- Moitinho, A., Vázquez, R. A., Carraro, G., Baume, G., Giorgi, E. E., & Lyra, W. 2006, *MNRAS*, 368, L77
- Momany, Y., Zaggia, S. R., Bonifacio, P., Piotto, G., De Angeli, F., Bedin, L. R., & Carraro, G. 2004, *A&A*, 421, L29
- Momany, Y. et al. 2005, *A&A*, 439, 111
- Momany, Y., Zaggia, S., Gilmore, G., Piotto, G., Carraro, G., Bedin, L. R., & de Angeli, F. 2006, *A&A*, 451, 515
- Monet, D. G. et al. 2003, *AJ*, 125, 984
- Ojha, D. K. 2001, *MNRAS*, 322, 426
- Pojmanski, G. 2002, *Acta Astronomica*, 52, 397
- Powell, W. L. J., Wilhelm, R., Carrell, K., & Westfall, A. 2008, [astro-ph/08031509](#)
- Press, W. H. et al. 2002, *Numerical recipes in C: the art of scientific computing* (3rd ed.; Cambridge, New York: Cambridge University Press)
- Preston, G. W., Sheckman, S. A., & Beers, T. C. 1991, *ApJ*, 375, 121
- Quinn, P. J., Hernquist, L., & Fullagar, D. P. 1993, *ApJ*, 403, 74
- Rey, S.-C., Yoon, S.-J., Lee, Y.-W., Chaboyer, B., & Sarajedini, A. 2001, *AJ*, 122, 3219
- Robin, A. C., Reylé, C., Derrière, S., & Picaud, S. 2003, *A&A*, 409, 523
- Rocha-Pinto, H. J., Majewski, S. R., Skrutskie, M. F., Patterson, R. J., Nakanishi, H., Muñoz, R. R., & Sofue, Y. 2006, *ApJ*, 640, L147
- Rucinski, S. M. 1993, *PASP*, 105, 1433
- Sandage, A., & Tammann, G. A. 2006, *ARA&A*, 44, 93
- Schlegel, D. J., Finkbeiner, D. P., & Davis, M. 1998, *ApJ*, 500, 525

- Siegel, M. H. 2006, *ApJ*, 649, L83
- Smith, H. A. 1995, *RR Lyrae stars* (Cambridge Astrophysics Series, Cambridge, New York: Cambridge University Press, —c1995)
- Sparke, L. S., & Casertano, S. 1988, *MNRAS*, 234, 873
- Stock, J. 1981, *Revista Mexicana de Astronomia y Astrofisica*, vol. 6, 6, 115
- Suntzeff, N. B., Kinman, T. D., & Kraft, R. P. 1991, *ApJ*, 367, 528
- Vivas, A. K. et al. 2001, *ApJ*, 554, L33
- Vivas, A. K. et al. 2004, *AJ*, 127, 1158
- Vivas, A. K., Zinn, R., & Gallart, C. 2005, *AJ*, 129, 189
- Vivas, A. K., & Zinn, R. 2006, *AJ*, 132, 714
- Vivas, K., Jaffe, Y. L., Zinn, R., Winnick, R., Duffau, S., & Mateu, C. 2008, *astroph/08071735*, *AJ* in press
- Wetterer, C. J., & McGraw, J. T. 1996, *AJ*, 112, 1046
- Zinn, R., & West, M. J. 1984, *ApJS*, 55, 45

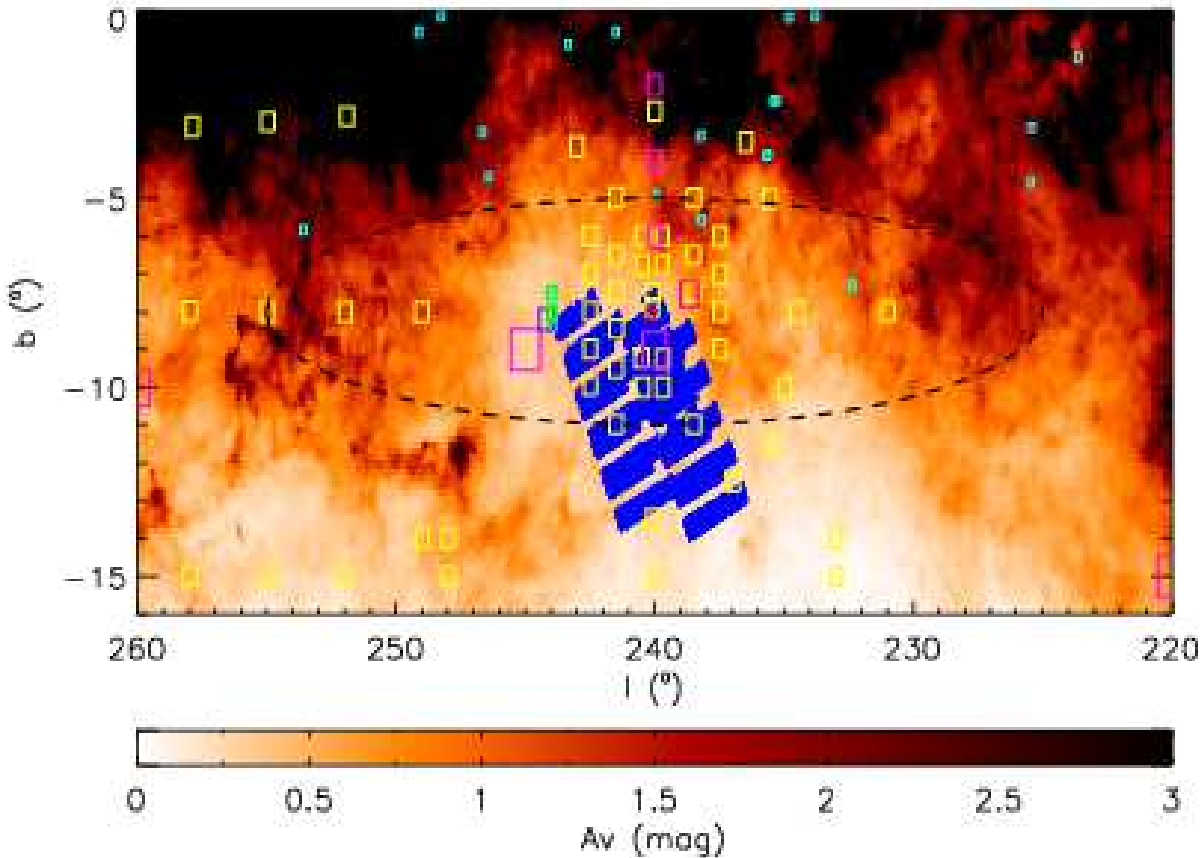


Fig. 1.— Schematic plot of the areas in CMA studied by different authors. The blue area shows the QUEST RRLS survey footprint. The colored rectangles represent the areas studied by Bellazzini et al 2006 (purple), Martinez-Delgado et al. 2005 (red), Carraro et al. 2005 and Moitinho et al. 2006 (cyan), Butler et al. 2007 and de Jong et al. 2007 (yellow), Conn et al. 2007 (magenta), Powell et al. 2008 (dark pink) and Carraro et al. 2008 (green). The axes of the dashed-lined ellipse are equal to the full-width at half maxima derived for CMA using an aspect ratio of 5 : 1 and the full-width at half maximum in the b direction measured by Butler et al. (2007). As noted by Butler et al. (2007), the aspect ratio of CMA could be larger than 5 : 1, in which case the ellipse would be more elongated in longitude. The colorscale represents the A_V values obtained from interpolation of the Schlegel et al. (1998) dust maps.

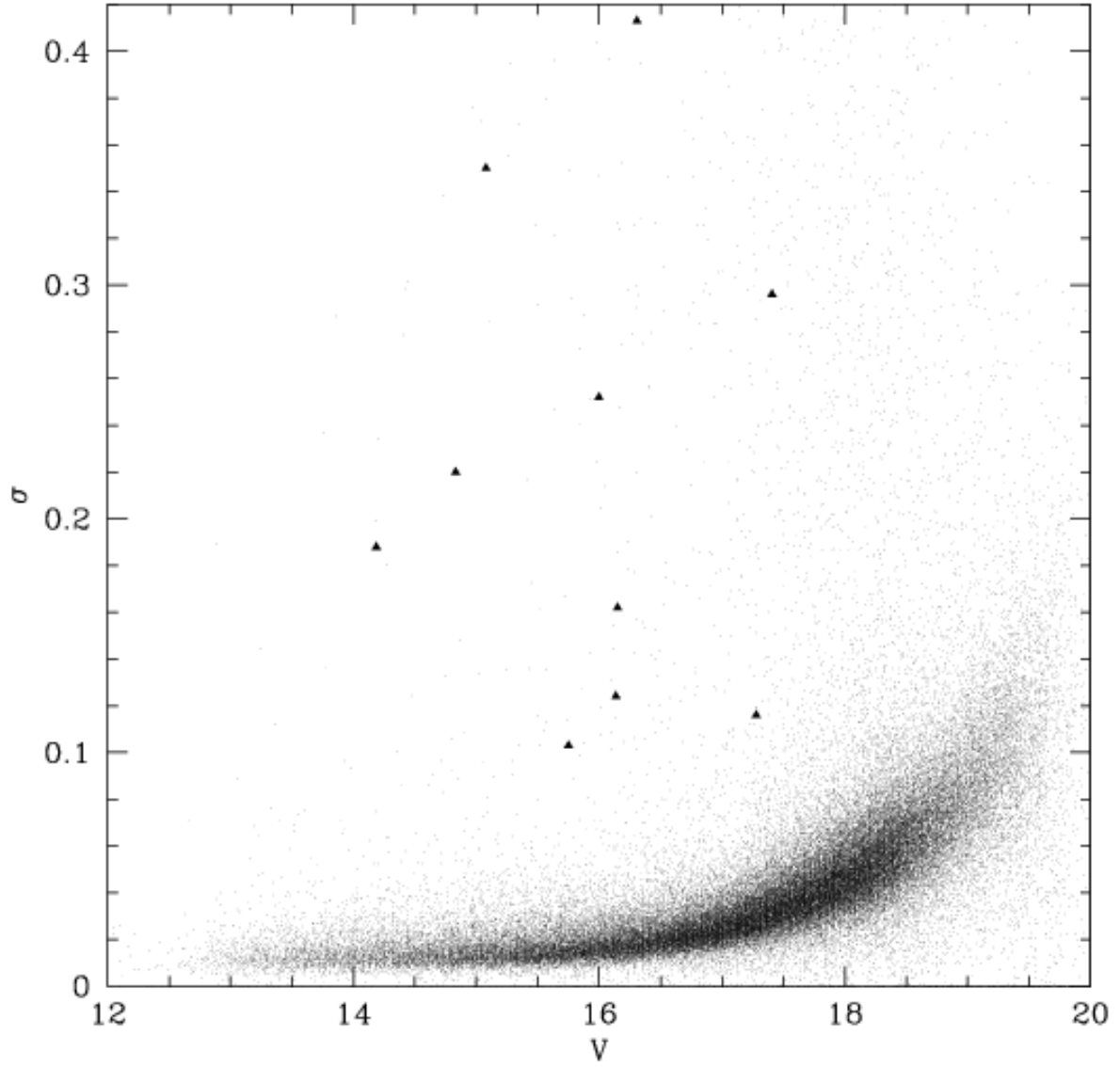


Fig. 2.— Typical standard deviation of PSF magnitudes versus mean magnitude, based in ~ 20 observations of ~ 80000 stars. Solid triangles represent the positions of the RRLS identified in this work.

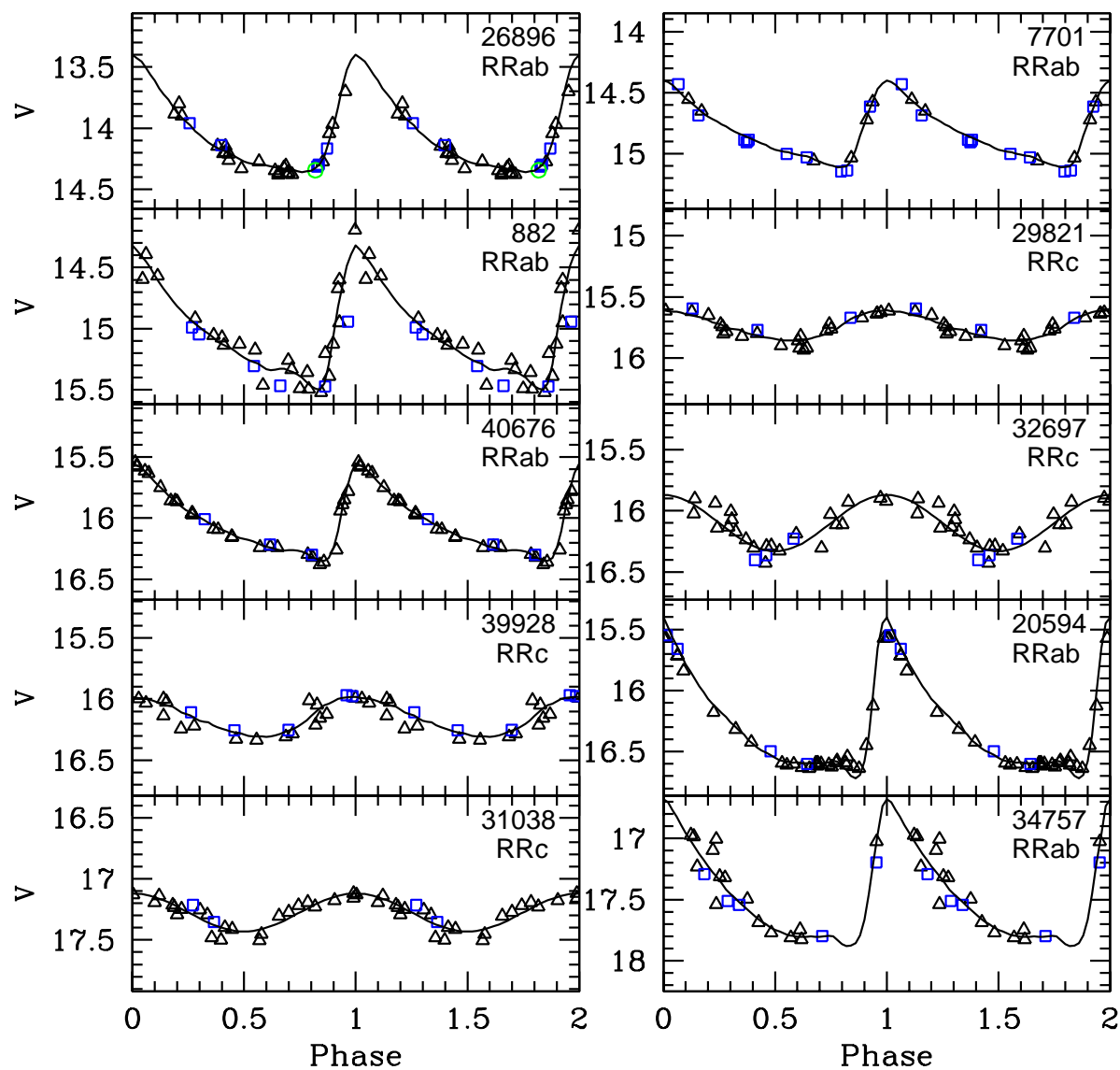


Fig. 3.— The light curves of the identified RRLs. Observations made with the QUEST camera are shown as open triangles, and follow-up observations from the SMARTS telescopes and the NOV 1.0m Reflector are shown with open squares and circles respectively. Solid lines show the best fitting template. Typical error bars are smaller than the symbol size.

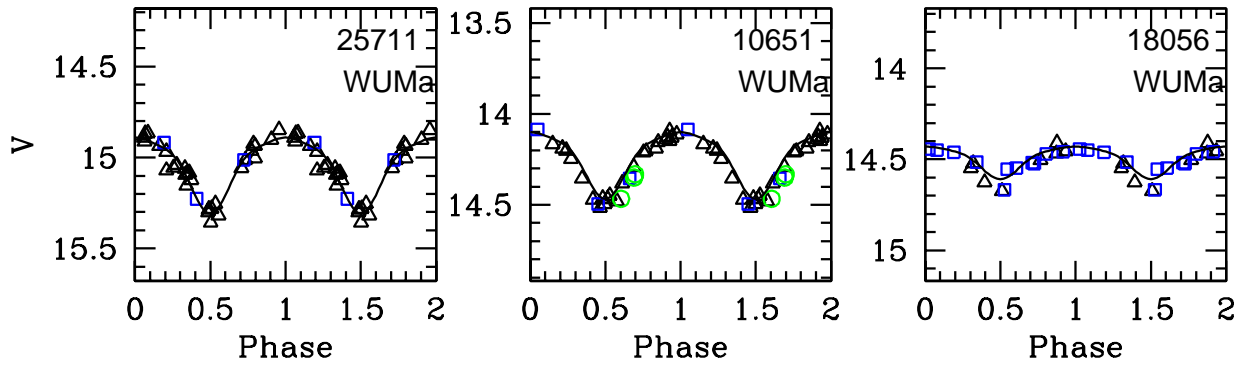


Fig. 4.— The light curves of the identified W UMa eclipsing contact binaries. Symbols are as in Fig. 3. Solid lines show the best fitting template.

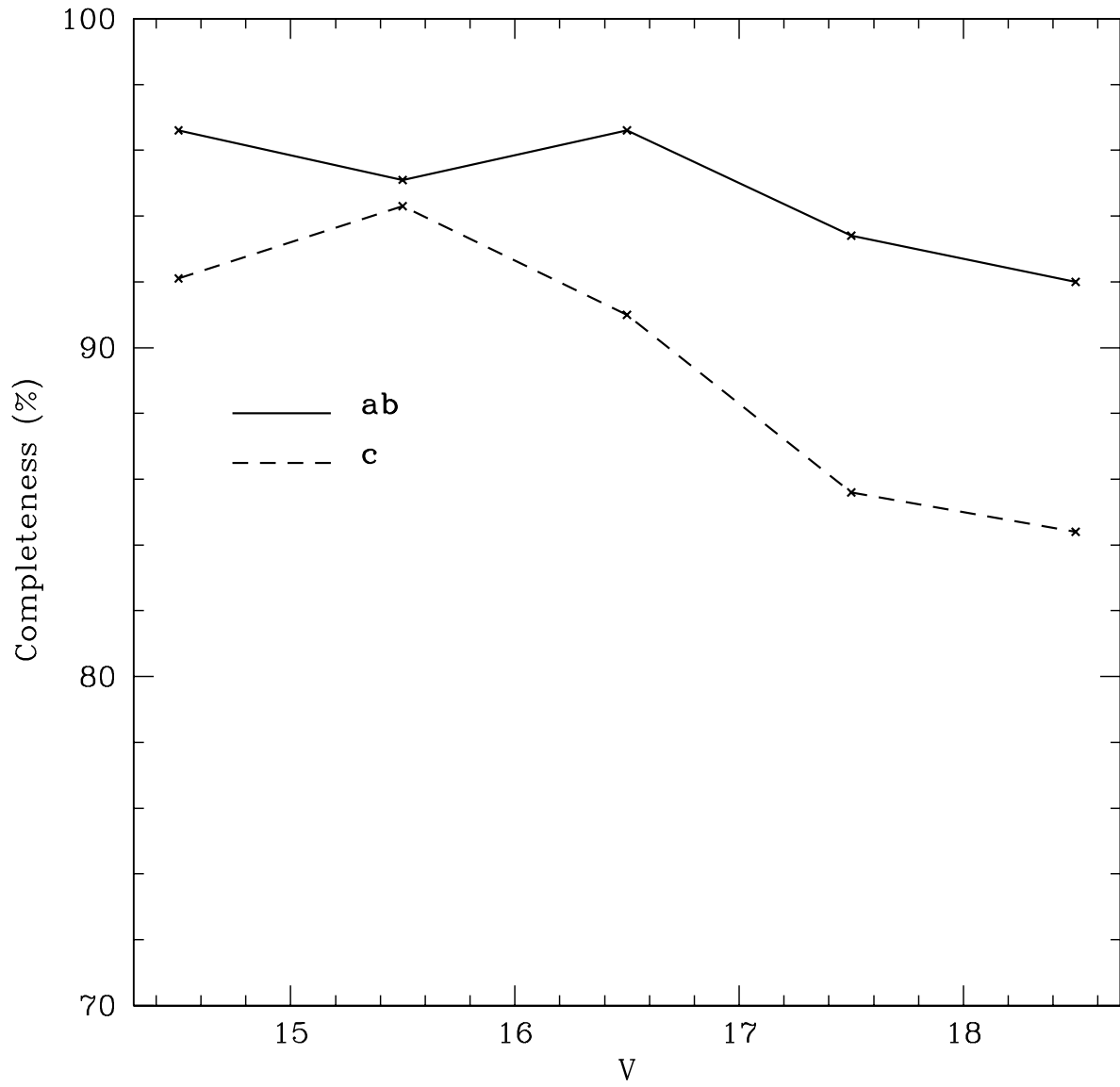


Fig. 5.— Completeness of the survey as a function of V magnitude.

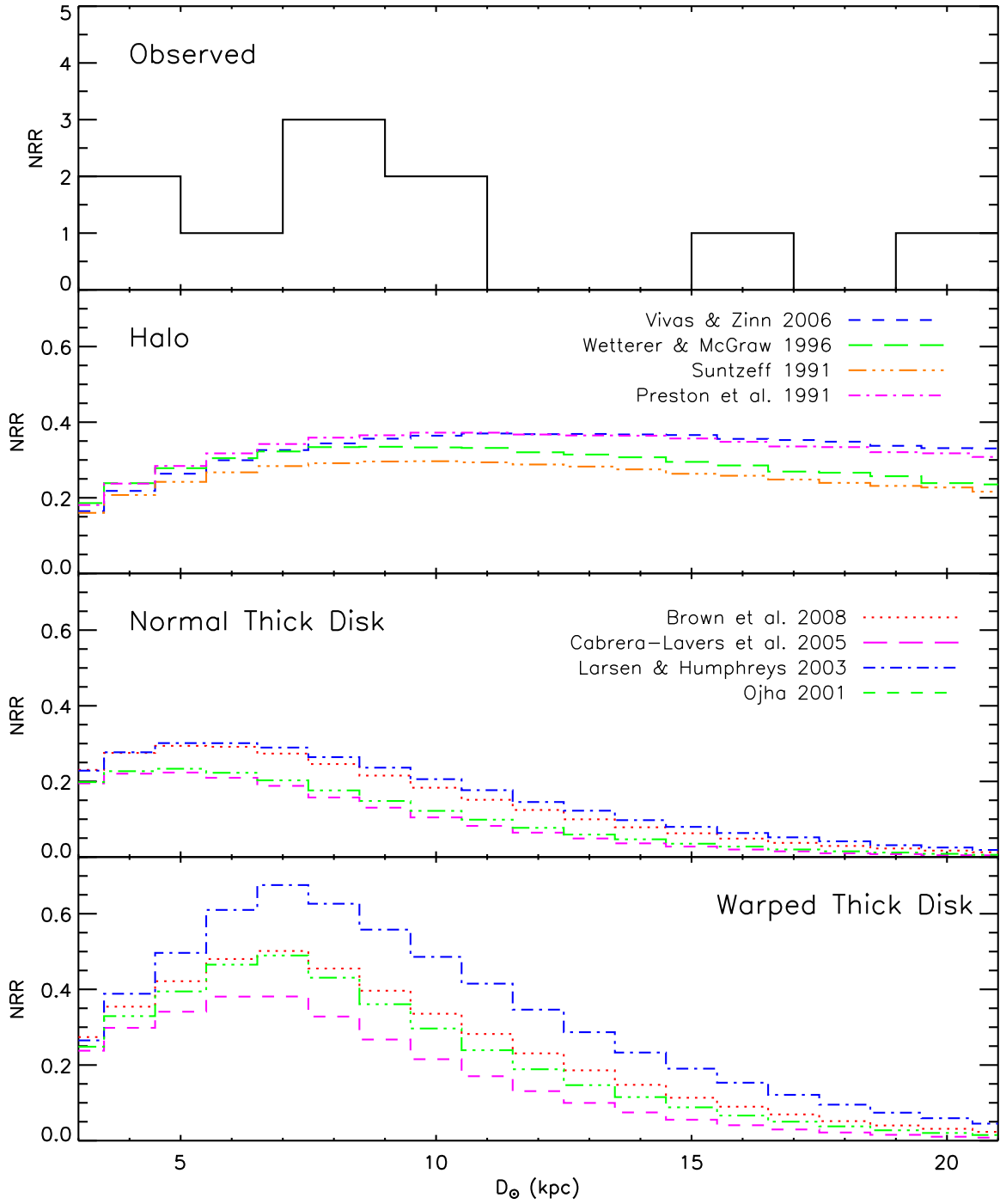


Fig. 6.— Observed and expected numbers of RRLS as a function of heliocentric distance. From top to bottom: Observed distribution, Galactic halo, normal thick disk and warped thick disk distributions.

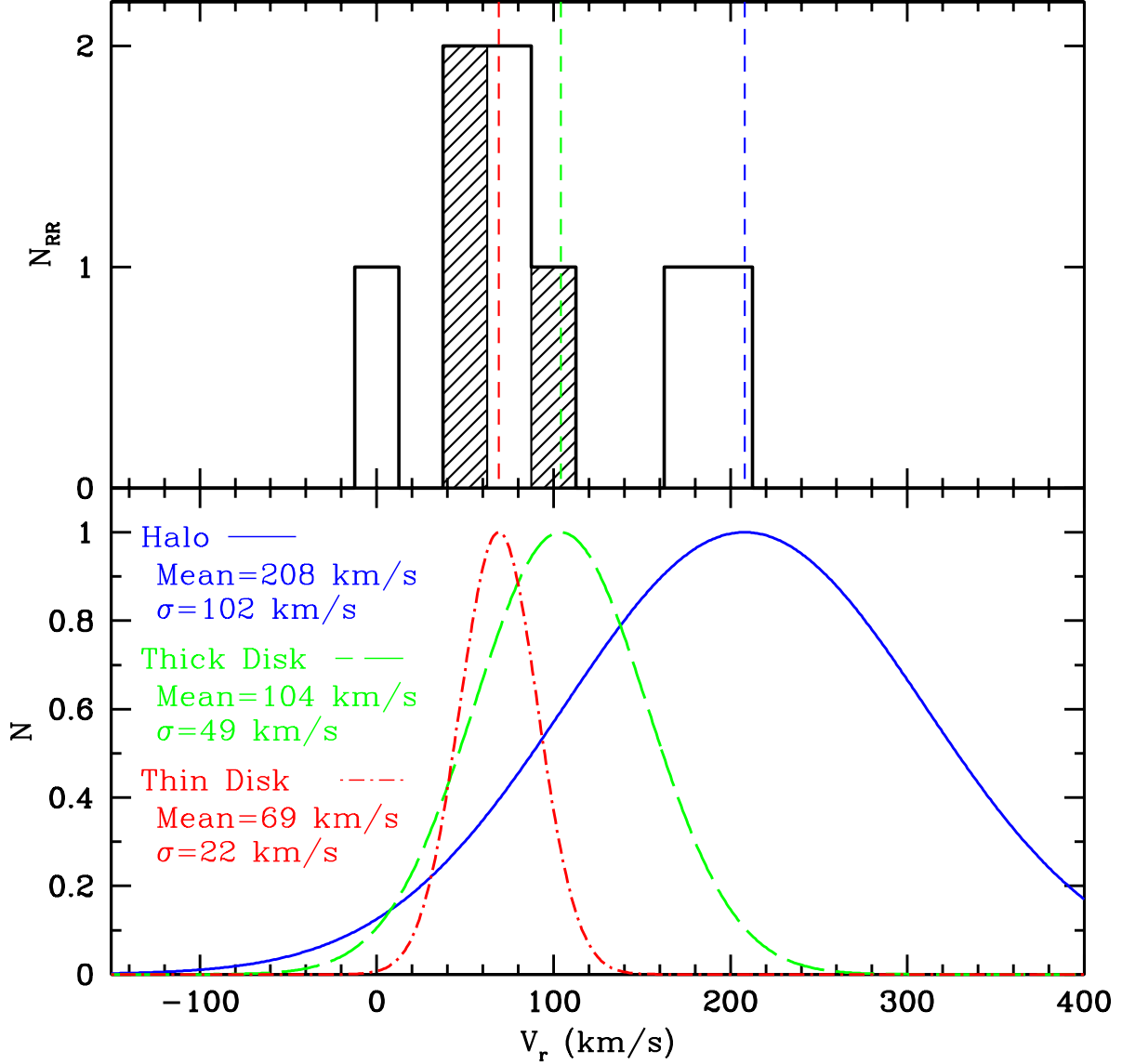


Fig. 7.— *Upper panel:* Radial velocity distribution of the 8 RRLS with $V < 16.5$. The shaded histogram corresponds to the radial velocity distribution of RRLc stars. *Bottom panel:* Radial velocity distributions of thin disk A-F stars (dashed dotted line), thick disk (dashed line) and halo (solid line) stars in the surveyed area, taken from the Besançon Galactic model (Robin et al. 2003). The dashed lines in the upper plot show the positions of the means of the distribution of each Galactic component.

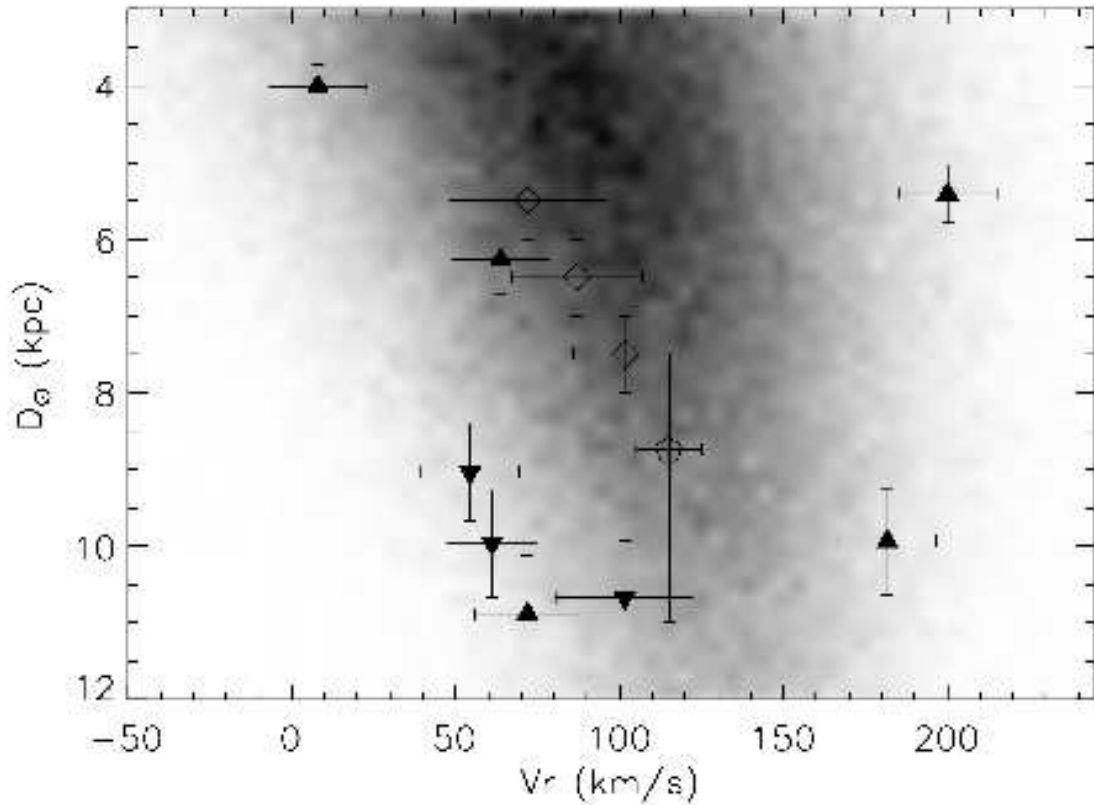


Fig. 8.— Heliocentric distance versus radial velocity of the 8 RRLS with $V < 16.5$. Solid triangles represent RRLS of type ab (up) and c (down). Open symbols represent RC (rhombuses) and RGB (pentagon) stars identified with the CMa overdensity Martin et al. (2005). The grayscale shows the distribution of thick disk stars in the surveyed area from the Besançon Galactic model (Robin et al. 2003). The distribution of halo stars in this diagram (not shown) has a broad peak in V_r at ~ 200 (see Fig. 8) and gentle falloff with D_{\odot} .

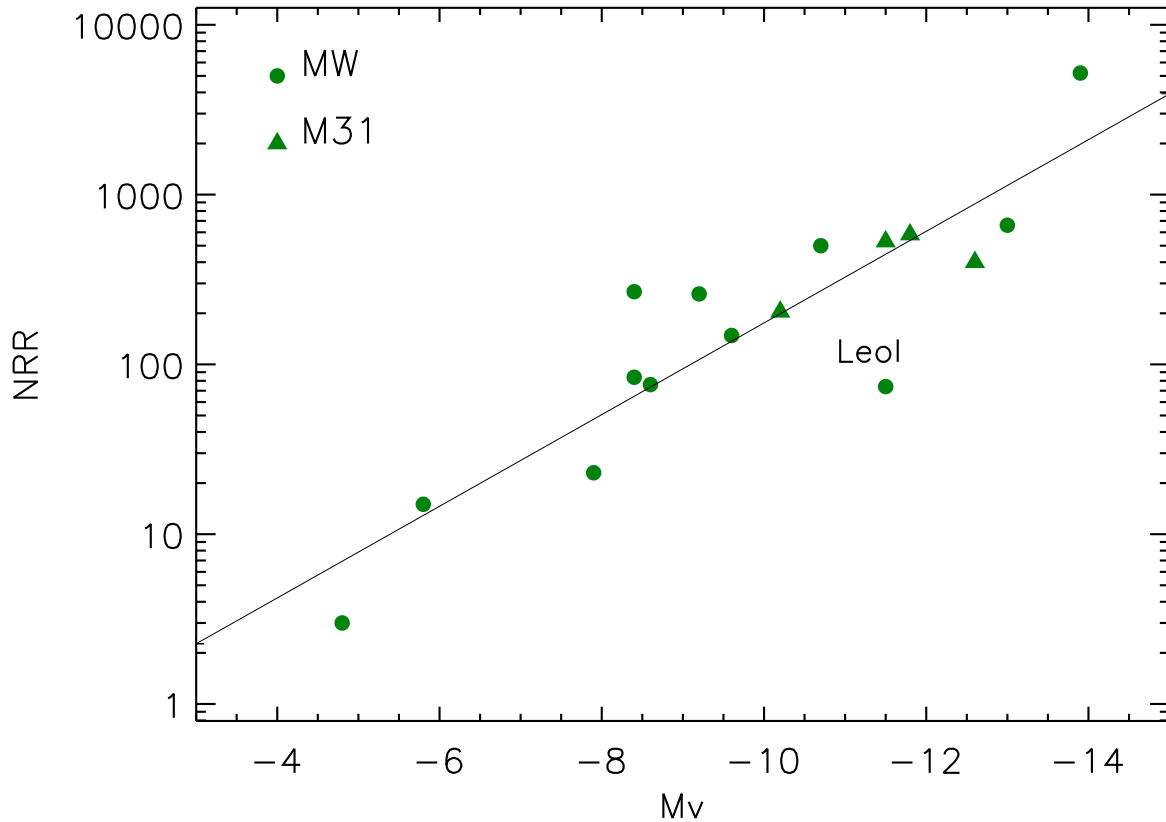


Fig. 9.— The observed number of RRLS in dSph satellites of the MW (*circles*) and M31 (*triangles*). A least squares fit to the data is represented by the straight line. Note that > 1000 RRLS are expected in the CMa dSph galaxy if it has $M_V \sim -14$ (Martin et al. 2004a; Bellazzini et al. 2004; Martínez-Delgado et al. 2005) and follows the trend in this diagram. The position of Leo I, the MW dSph galaxy with the lowest S_{RR} (see §4), is marked.

Table 1. Summary of previous stellar population studies conducted in CMa.

Tracer	Age (Gyrs)	[Fe/H]	D_{\odot} (kpc)	Technique	Filters	Interpretation	Reference
Blue Plume	1 – 2	MS-fitting	BV	dSph galaxy	B04
Blue Plume	$\sim 0.7 - 2$	-0.3 or ~ -1.0	~ 7.5 or 9.3	HD modelling	BR	dSph galaxy	dJ07
Blue Plume	$\lesssim 0.1$...	10.8	TCDs, MS-fitting	UBVRI	Spiral arm	C05, Moi06
Blue Plume	...	-0.37 to -0.5	6.0 ± 2.7	TCDs, spectroscopy	UBV	Spiral arm	P08
B5-A0 stars	$\lesssim 0.1$...	$9.8^{+1.5}_{-1.0}$	TCDs	UBVRI	Spiral arm	C08
MS	3 – 6	$\sim -1.0 \pm 0.1$	~ 7.5	HD modelling	BR	dSph galaxy	dJ07, B07
RGB, MS	4 – 10	-0.66 to -0.35	$\sim 8.1 \pm 1.2$	Isocrone fitting	BV	dSph galaxy	B04
M-giants	4 – 10	$-1.0 < [M/H]$	7.1 ± 0.1	CMD fitting	JHK	dSph galaxy	M04
RGB, RC	5.5 to 8.5	Spectroscopy	...	dSph galaxy	M05
F-G-K stars	6 ± 2	$\sim -0.3 \pm 0.3$	6	TCDs	UBVRI	Warped Thick Disk	C08

References. — B04=Bellazzini et al. (2004), M04=Martin et al. (2004a), M05=Martin et al. (2005), C05=Carraro et al. (2005), Moi06=Moitinho et al. (2006), B07=Butler et al. (2007), dJ07=de Jong et al. (2007), C08=Carraro et al. (2008), P08=Powell et al. (2008)

Table 2. Light curve and physical parameters of RRLS.

ID	α (deg)	δ (deg)	N	Period (d)	Amp_V	Type	HJD_{max} 2450000 d	$\langle V_0 \rangle$	D_\odot (kpc)	V_γ (km s^{-1})	σV_γ (km s^{-1})	[Fe/H]
7701	108.429950	-28.128540	16	0.58446	0.71	RRab	3260.75930	14.22	5.4	200	15	-1.51
882	104.492882	-27.708120	29	0.46353	1.18	RRab	3372.89115	14.54	6.3	64	15	-1.52
20594	105.830994	-27.565201	35	0.50893	1.32	RRab	3372.41209	15.73	10.9	72	16	-1.83
26896	108.468697	-29.726669	29	0.39725	0.96	RRab	3372.85468	13.57	4.0	8	15	-1.29
29821	108.591827	-31.073851	25	0.37719	0.25	RRc	3372.83819	15.33	9.0	54	15	-1.27
31038	107.737091	-27.722931	25	0.26672	0.31	RRc	3372.95514	16.73	17.2
32697	107.872360	-27.761780	25	0.20140	0.46	RRc	3372.81509	15.54	10.0	61	14	-1.26
34757	109.645363	-29.783131	20	0.54532	1.20	RRab	3372.59181	17.09	20.3
39928	109.702118	-30.578770	22	0.33740	0.33	RRc	3372.86688	15.69	10.7	102	21	-0.78
40676	107.920067	-28.308350	31	0.57517	0.80	RRab	3373.13496	15.54	9.9	182	15	-1.44

Table 3. Light curve parameters of rejected RRLS candidates.

ID	α (deg)	δ (deg)	N	Period (d)	V_{amp}	HJD_{max} 2450000 d	$\langle V_0 \rangle$	Reason for Rejection
5564	105.416870	-28.277680	22	0.29700	0.17	3258.68871	15.69	late-F spectra
10651	105.439903	-31.074100	30	0.37339	0.37	3372.46691	13.88	W UMa
25711	105.681969	-28.129801	32	0.42189	0.42	3372.97294	15.03	W UMa
6460	107.042080	-27.251020	22	0.21343	0.29	3259.82428	14.49	late-F spectra
18056	107.396880	-28.883540	19	0.27842	0.17	3259.93843	14.10	W UMa
17237	108.275560	-26.897120	17	0.24430	0.24	3259.75716	14.36	late-F spectra

Table 4. Density profiles of the Galactic halo and thick disk.

		$\rho(\vec{r})$
Halo		$\rho_{\odot}^{RR} \left(\frac{1}{R_{\odot}} \sqrt{x^2 + y^2 + \left(\frac{z}{c/a}\right)^2} \right)^n$
Thick Disk		$\rho_{\odot}^{RR} \exp\left(-\frac{R_{gal}-R_{\odot}}{h_R}\right) \exp\left(-\frac{ z }{h_z}\right)$
Warped		$\rho_{\odot}^{RR} \exp\left(-\frac{R_{gal}-R_{\odot}}{h_R}\right) \exp\left(-\frac{ z-z_w }{h_z}\right)$
Thick Disk		with $z_w=[C_w R_{gal}(\text{pc})^{\varepsilon_w} \sin(\phi-\phi_w)-15]\text{pc}$ if $R_{gal}<13\text{kpc}$ with $z_w=z_w(13\text{kpc})$ if $R_{gal}>13\text{kpc}$

Note. — In the table, x, y, z are cartesian Galactocentric coordinates, $R_{\odot} = 8$ kpc is the distance from the Sun to the Galactic center and R_{gal} the Galactocentric distance along the plane. In the density profile assumed for a warped thick disk, $C_w = 2.1 \times 10^{-19}\text{pc}$, $\varepsilon_w = 5.25$ and $\phi_w = -5^\circ$, are the warp parameters according to López-Corredoira et al. (2002).

Table 5. Number of RRLS expected in each Galactic component.

	Reference	$\rho_{\odot}^{RR} (\frac{\#}{kpc^3})$	n	(c/a)	Tracer	N_{RR}	
Halo	Vivas & Zinn (2006)	$4.2^{+0.5}_{-0.4}$	-3.1 ± 0.1	Variable	RRLS	6	
	Wetterer & McGraw (1996)	5.3 ± 2	-3.53 ± 0.08	Variable	RRLS	4	
	Preston et al. (1991)	4.8	-3.2 ± 0.1	Variable	RRLS	6	
	Suntzeff et al. (1991)	4.5 ± 1	-3.5	1	RRLS	5	
	Reference	$\rho_{\odot}^{RR} (\frac{\#}{kpc^3})$	h_z (pc)	h_R (kpc)	Tracer	N_{RR}^{normal}	N_{RR}^{warped}
Thick	Brown et al. (2008)	...	1026 ± 100	3.5 ± 0.5	BHB stars	3	5
Disk	Cabrera-Lavers et al. (2005)	...	1061 ± 52	3.04 ± 0.11	2MASS RC stars	2	3
	Larsen & Humphreys (2003) [†]	...	900 ± 65	4.7 ± 0.2	Star counts	3	6
	Ojha (2001)	...	860 ± 200	$3.7^{+0.8}_{-0.5}$	2MASS star counts	2	4

Note. — The symbol N_{RR} represents the number of RRLS in the distance range from 3 to 20 kpc, both for the halo and normal/warped thick disk. [†]For the scale-height Larsen & Humphreys (2003) obtained $h_z = 870 - 930 \pm 50 - 80pc$, for the present study we use the intermediate value reported here.